FAS-RIS: A Block-Correlation Model Analysis

Xiazhi Lai, Junteng Yao, Kangda Zhi, Tuo Wu,
David Morales-Jimenez, *Senior Member*, *IEEE*, and Kai-Kit Wong, *Fellow*, *IEEE*

***Abstract*—In this correspondence, we analyze the performance of a reconfigurable intelligent surface (RIS)-aided communication system that involves a fluid antenna system (FAS)-enabled receiver. By applying the central limit theorem (CLT), we derive approximate expressions for the system outage probability when the RIS has a large number of elements. Also, we adopt the block-correlation channel model to simplify the outage probability expressions, reducing the computational complexity and shedding light on the impact of the number of ports. Numerical results validate the effectiveness of our analysis, especially in scenarios with a large number of RIS elements.**

***Index Terms*—Fluid antenna system (FAS), outage probability, reconfigurable intelligent surface (RIS).**

I. Introduction

FLUID antenna system (FAS) has emerged as a crucial technology for next-generation wireless communications. This importance arises because traditional fixed antenna techniques, e.g., multiple-input-multiple-output (MIMO), are constrained by the physical size of wireless devices, whereas FAS enables flexible switching of finely-positioned elements to the most desirable port, e.g., [1], [2], [3], [4]. In practice, FAS can be implemented via pixel-based [5] or liquid metal structures [6]. The optimal port can be determined using learning-based methods exploiting spatial correlation [7], [8]. FAS has made an active research topic recently, see e.g., [9], [10], [11], [12], [13], [14], [15]. An overview article can be found in [16].

To study the achievable performance of FAS-enabled systems, accurate while tractable channel models are necessary. Considering this, a simplified channel model was originally used in [17], [18]. This model approximates the effect of port correlation using a single correlation parameter. A more accurate eigenvalue-based channel model was subsequently proposed in [19]. Due to mathematical difficulty, performance analysis based on this model is, however, a challenge. This was recently overcome by the new block-correlation model recently developed in [20], which is favorable for insightful analysis of FAS-assisted communications.

On the other hand, research on reconfigurable intelligent surface (RIS) is going strong. RIS is particularly important in deep-fading scenarios where obstacles such as thin walls may obstruct the direct link between the transmitter and receiver [21], [22]. RIS in a sense re-establishes the line-of-sight (LoS) link between the transmitter and receiver when it is blocked by modifying the phases of the reflected signals. Recent efforts have seen the benefits of RIS in terms of coverage probability in [23], and [24] also considered the use of RIS in the presence of multiple users, in terms of ergodic capacity.

Integrating the capabilities of FAS and RIS presents a robust approach to enhance wireless communication performance, so the synergy of FAS and RIS offers a promising direction for advancing communication systems. However, the performance of FAS-RIS is not well understood, and remains unexplored. Motivated by this, this correspondence explores a RIS-assisted communication system that includes a FAS-enabled receiver. Here, FAS is used to improve the quality of received signals, while RIS is employed to re-establish the LoS link when it is originally blocked. Using the central limit theorem (CLT), we derive the system outage probability when the number of RIS elements is large. Also, the block-correlation approximation technique in [20] is adopted to achieve simplified expressions for the outage probability. Our numerical results validate our analysis and reveal great potential of FAS and RIS.

Notations: $X \sim \mathcal{CN}(\alpha, \beta)$ represents a complex Gaussian random variable (RV) with mean α and variance β. $\mathbf{E}(\cdot)$ and $\mathbf{Var}(\cdot)$ denote, respectively, the expectation and variance of a RV. Additionally, $f_X(x)$ and $F_X(x)$ denote the probability density function (PDF) and cumulative distribution function (CDF) of the RV, X, respectively.

II. System Model

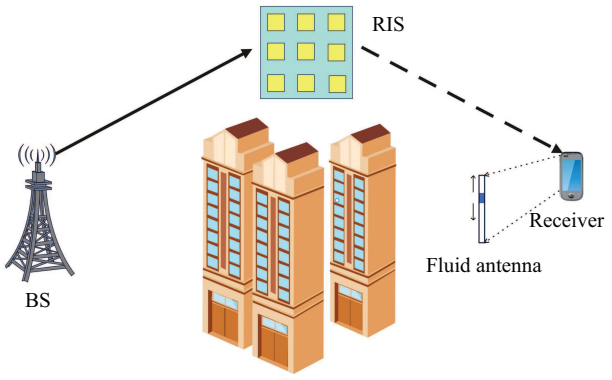

Fig. 1. A RIS-assisted communication system with a FAS-enabled user.

As depicted in Fig. 1, a RIS-assisted communication system is considered. The communication system consists of a base station (BS) equipped with a single fixed-position antenna, a RIS with M reflecting elements, and a receiver equipped a fluid antenna capable of switching among N ports within a linear space of $W\lambda$, where W is the normalized size, and λ

X. Lai is with the School of Computer Science, Guangdong University of Education, Guangzhou, Guangdong, China (E-mail: xzlai@outlook.com).

J. Yao is with the Faculty of Electrical Engineering and Computer Science, Ningbo University, Ningbo 315211, China (E-mail: yaojunteng@nbu.edu.cn).

K. Zhi and T. Wu are with the School of Electronic Engineering and Computer Science at Queen Mary University of London, London E1 4NS, U.K. (Email: {tuo.wu, k.zhi}@qmul.ac.uk).

D. Morales-Jimenez is with Department of Signal Theory, Networking and Communications, Universidad de Granada, Granada 18071, Spain (Email: dmorales@ugr.es).

K.-K. Wong is with the Department of Electronic and Electrical Engineering, University College London, WC1E 6BT London, U.K., and also with the Yonsei Frontier Laboratory and the School of Integrated Technology, Yonsei University, Seoul 03722, South Korea (e-mail: kai-kit.wong@ucl.ac.uk).

is the carrier wavelength. Here, the BS transmits the signal to the receiver aided by the RIS, and the direct link between the BS and the receiver is assumed broken. It is also assumed that the time delay for port switching is negligibly small.

A. Communication Model

Given the absence of the direct link between the BS and the receiver, the receiver relies on the signals solely from the reflections of the RIS. Consequently, at the k-th FAS port of the user, the received signal is given by [23]

$$y_k = \sqrt{P_S}\sum_{m=1}^{M} h_m v_{m,k} e^{-2i\pi\theta_m} s + n_k, \tag{1}$$

where $h_m \sim \mathcal{CN}(0,\epsilon_1)$ denotes the complex channel coefficient from the BS to the m-th RIS element, and $v_{m,k} \sim \mathcal{CN}(0,\epsilon_2)$ denotes the channel from the m-th RIS element to the k-th FAS port, $s \sim \mathcal{CN}(0,1)$ is the transmit signal, P_S is the transmit power, $n_k \sim \mathcal{CN}(0,\sigma_n^2)$ is the additional white Gaussian noise, θ_m denotes the reflecting phase of the m-th RIS element, and the RIS is assumed to have full knowledge of the phases of h_m and $v_{m,k}$; thus can adjust θ_m to maximize the channel gain, i.e., $\theta_m = -\arg(h_m v_{m,k})$. Follow this, the combined channel at the n-th FAS port can be expressed as

$$\gamma_k = \sum_{m=1}^{M} |h_m||v_{m,k}|. \tag{2}$$

It can be readily observed that both $|h_m|$ and $|v_{m,k}|$ follow Rayleigh distribution, $\mathbf{E}(|h_m||v_{m,k}|) = \mathbf{E}(|h_m|)\mathbf{E}(|v_{m,k}|) = \pi\sqrt{\epsilon_1\epsilon_2}/4$, and $\mathbf{Var}(|h_m||v_{m,k}|) = \mathbf{E}(|h_m|^2|v_{m,k}|^2) - (\mathbf{E}(|h_m||v_{m,k}|))^2 = \epsilon_1\epsilon_2(1-\pi^2/16)$.

At the FAS, the port with the maximum channel gain will be selected for receiving the signal. Consequently, the resulting channel at the optimal port is written as

$$\gamma^* = \max_{k\in\{1,2,\ldots,N\}} \gamma_k. \tag{3}$$

B. FAS Channel Correlation Model

For the correlation between two different ports of the FAS, the 3D Clarke's model is adopted. Specifically, the correlation coefficient between ports k and l is modeled by

$$g_{k,l} = \mathrm{sinc}\left(\frac{2\pi(k-l)W}{N-1}\right), \tag{4}$$

where $\mathrm{sinc}(x) = \dfrac{\sin(x)}{x}$. Note that $\mathrm{sinc}(x)$ is an odd function, which indicates that the correlation coefficient matrix of $\mathbf{v}_m = [v_{m,1},\ldots,v_{m,N}]$ is a Toeplitz matrix as

$$\begin{aligned}\mathbf{\Sigma} \in \mathbb{R}^{N\times N} &= \mathbf{topelitz}(g_{1,1}, g_{1,2}, \ldots, g_{1,N}) \\ &= \begin{pmatrix} g_{1,1} & g_{1,2} & \cdots & g_{1,N} \\ g_{1,2} & g_{1,1} & \cdots & g_{1,N-1} \\ \vdots & & \ddots & \vdots \\ g_{1,N} & g_{1,N-1} & \cdots & g_{1,1} \end{pmatrix}.\end{aligned} \tag{5}$$

III. Outage Performance Analysis

In this section, the outage performance of the system is analyzed. First, let us denote R as the target transmission rate, and the outage probability is accordingly given as

$$\begin{aligned}P_{\text{out}} &= F_{\gamma^*}(\Lambda_{\text{th}}) = \Pr\left(\log_2\left(1+\frac{P_S(\gamma^*)^2}{\sigma_n^2}\right) \le R\right) \\ &= F_{\gamma^*}(\Lambda_{\text{th}}),\end{aligned} \tag{6}$$

where $\Lambda_{\text{th}} = ((2^R-1)\sigma_n^2/P_S)^{1/2}$. To proceed with the outage probability analysis, it is necessary to derive the approximation CDF of γ^*, i.e., $F_{\gamma^*}(y)$. Given that the exact expression for $F_{\gamma^*}(y)$ is intractable, the following subsections will develop several approximations for $F_{\gamma^*}(y)$.

A. CLT Approximation

In practice, the number of RIS elements, M, is supposed to be very large, and thus the CLT can be applied. Consequently, $\mathbf{\Gamma} = [\gamma_1,\ldots,\gamma_N]$ can be approximated by $\bar{\mathbf{\Gamma}} = [\bar{\gamma}_1,\ldots,\bar{\gamma}_N]$. That is, the PDF and CDF of $\mathbf{\Gamma}$ are similar to those of $\bar{\mathbf{\Gamma}}$. Furthermore, the mean and variance of $\bar{\gamma}_k$ are identical to those of γ_k, which can be computed as

$$E_\gamma = M\mathbf{E}(|h_m||v_{m,k}|) = \frac{M\pi\sqrt{\epsilon_1\epsilon_2}}{4}, \tag{7}$$

$$V_\gamma = M\mathbf{Var}(|h_m||v_{m,k}|) = M\epsilon_1\epsilon_2\left(1-\frac{\pi^2}{16}\right). \tag{8}$$

Moreover, as γ_k for $k=1,\ldots,N$ share the same $|h_m|$ for $m=1,\ldots,M$, and $|v_{m,k}|$ are correlated for different k, it can be easily demonstrated that $\bar{\gamma}_k$ for $k=1,\ldots,N$ are correlated. Hence, given the calculation of Pearson correlation coefficient and (2), the correlation coefficient between γ_k and γ_l can be formulated as

$$\eta(g_{k,l}) = \frac{\mathbf{E}(\gamma_k\gamma_l) - E_\gamma^2}{V_\gamma} = \frac{M\epsilon_1\mathbf{E}(|v_{m,k}||v_{m,l}|) - E_\gamma^2/M}{V_\gamma}, \tag{9}$$

where

$$\mathbf{E}(|v_{m,k}||v_{m,l}|) = \int_0^\infty\int_0^\infty xy f_{|v_{m,k}|,|v_{m,l}|}(x,y)dxdy, \tag{10}$$

and $f_{|v_{m,k}|,|v_{m,l}|}(x,y)$ is the joint PDF of RVs $|v_{m,k}|$ and $|v_{m,l}|$, which is given by

$$\begin{aligned}f_{|v_{m,k}|,|v_{m,l}|}(x,y) = \frac{4x^2y^2}{\epsilon_2^2(1-g_{k,l})} e^{-\frac{x^2}{\epsilon_2}} e^{-\frac{y^2+g_{k,l}x^2}{\epsilon_2^2(1-g_{k,l})}} \\ \times I_0\left(\frac{2g_{k,l}xy}{\epsilon_2(1-g_{k,l})}\right),\end{aligned} \tag{11}$$

in which $I_0(\cdot)$ denotes the zeroth order of Bessel function of the first kind. Note that $\mathbf{E}(|v_{m,k}||v_{m,l}|)$ can be computed via numerical integration.

Based on the correlation coefficient in (9), we can formulate the correlation coefficient matrix of $\bar{\mathbf{\Gamma}}$ as

$$\mathbf{\Omega} \in \mathbb{R}^{N\times N} = \mathbf{toeplitz}\left(\eta(g_{1,1}),\ldots,\eta(g_{1,N})\right), \tag{12}$$

and the joint PDF of $\bar{\mathbf{\Gamma}}$ is written as

$$f_{\gamma_1,\ldots,\gamma_N}(x_1,\ldots,x_N) = \frac{e^{-\frac{1}{2}(\mathbf{X}-\mathbf{E}_\gamma)^T(V_\gamma\cdot\mathbf{\Omega})^{-1}(\mathbf{X}-\mathbf{E}_\gamma)}}{(2\pi V_\gamma)^{N/2}(\det\mathbf{\Omega})^{1/2}}, \tag{13}$$

where

$$\mathbf{X} = [x_1, \ldots, x_N]^T, \text{ and } \mathbf{E}_\gamma = [E_\gamma, \ldots, E_\gamma]^T. \quad (14)$$

Utilizing the PDF of $\bar{\mathbf{\Gamma}}$ in (13), the CDF of RV, $\bar{\gamma}^*$, can be expressed via the joint CDF of N-dimensional Gaussian distribution, i.e., $\Phi(y, V_\gamma \cdot \mathbf{\Omega}, E_\gamma)$, as

$$\begin{aligned} &F_{\bar{\gamma}^*}(y) \\ &= \Phi(y, V_\gamma \cdot \mathbf{\Omega}, E_\gamma) \\ &= \underbrace{\int_{-\infty}^{y} \cdots \int_{-\infty}^{y}}_{N} f_{\gamma_1,\ldots,\gamma_N}(x_1, \ldots, x_N) dx_1 \cdots dx_N, \end{aligned} \quad (15)$$

where the calculation of $\Phi(y, V_\gamma \cdot \mathbf{\Omega}, E_\gamma)$ can be implemented via mathematical tools, such as Matlab and Maple. However, for large values of N, say $N \geq 25$, the complexity of the calculation of $F_{\bar{\gamma}^*}(y)$ is prohibitive as an N-dimensional integral is required. To overcome the difficulty, we will provide approximate expressions of $F_{\bar{\gamma}^*}(y)$ in the next subsections.

B. Block-Correlation Channel Approximation

In this part, we resort to a block-correlation approximation model in [20]. That is, the random vector $\mathbf{v}_m$ can be approximated by $\bar{\mathbf{v}}_m$, and the the correlation coefficient matrix of $\bar{\mathbf{v}}_m$ can be presented in the following form:

$$\hat{\mathbf{\Sigma}} \in \mathbb{R}^{N\times N} = \begin{pmatrix} \mathbf{A}_1 & \mathbf{0} & \cdots & \mathbf{0} \\ \mathbf{0} & \mathbf{A}_2 & \cdots & \mathbf{0} \\ \vdots & & \ddots & \vdots \\ \mathbf{0} & \mathbf{0} & \cdots & \mathbf{A}_D \end{pmatrix}, \quad (16)$$

where

$$\mathbf{A}_d \in \mathbb{R}^{L_d\times L_d} = \begin{pmatrix} 1 & \mu & \cdots & \mu \\ \mu & 1 & \cdots & \mu \\ \vdots & & \ddots & \vdots \\ \mu & \mu & \cdots & 1 \end{pmatrix}, \quad (17)$$

μ denotes a constant close to 1, and $\sum_{L_d=1}^{D} L_d = N$ with $D = |S\{\lambda_{th}\}|$ being determined by the number of principal eigenvalues of $\mathbf{\Sigma}$. That is, there exists $S\{\lambda_{\text{th}}\} = \{\lambda_n | \lambda_n \geq \lambda_{\text{th}}, n = 1, \ldots, N\}$, and D equals to the cardinal number of $S\{\lambda_{th}\}$, where λ_{th} is a small number to ensure that enough eigenvalues are included in $S\{\lambda_{\text{th}}\}$, which can be dynamically adjusted. Also, L_b is determined by

$$\underset{L_1,\ldots,L_B}{\arg\min} \ \text{dist}(\hat{\mathbf{\Sigma}}, \mathbf{\Sigma}), \quad (18)$$

where $\text{dist}(\cdot)$ is a distance metric between two matrices, which is determined by the difference of their eigenvalues and the detailed procedure can be found in [20].

Based on the block-correlation model, we can approximate $\mathbf{\Gamma}$ with $\hat{\mathbf{\Gamma}} = [\hat{\gamma}_1, \ldots, \hat{\gamma}_N]$. Applying the Pearson correlation coefficient calculation, the correlation coefficient matrix of $\hat{\mathbf{\Gamma}}$ is given as

$$\hat{\mathbf{\Omega}} \in \mathbb{R}^{N\times N} = \begin{pmatrix} \mathbf{B}_1 & \mathbf{C} & \cdots & \mathbf{C} \\ \mathbf{C} & \mathbf{B}_2 & \cdots & \mathbf{C} \\ \vdots & & \ddots & \vdots \\ \mathbf{C} & \mathbf{C} & \cdots & \mathbf{B}_D \end{pmatrix}, \quad (19)$$

where all the elements in the submatrix within $\mathbf{C}$ are given as $\rho_0 = \eta(0)$, and

$$\mathbf{B}_d \in \mathbb{R}^{L_d\times L_d} = \begin{pmatrix} 1 & \rho_1 & \cdots & \rho_1 \\ \rho_1 & 1 & \cdots & \rho_1 \\ \vdots & & \ddots & \vdots \\ \rho_1 & \rho_1 & \cdots & 1 \end{pmatrix}, \quad (20)$$

where $\rho_1 = \eta(\mu)$.

Based on the structure of the correlation coefficient matrix $\hat{\mathbf{\Gamma}}$, we can then rearrange the subscript and rewrite $\hat{\mathbf{\Gamma}}$ into $[\hat{\gamma}_{1,1}, \ldots, \hat{\gamma}_{L_1,1}, \ldots, \hat{\gamma}_{k,d}, \ldots, \hat{\gamma}_{L_D,D}]$. Here, $\hat{\gamma}_{k,d}$ can be reformulated as

$$\begin{aligned} \hat{\gamma}_{k,d} =& \sqrt{1-\rho_1} z_{2,k,d} + \sqrt{\rho_1 - \rho_0} z_{1,d} + \sqrt{\rho_0} z_0 + E_\gamma \\ =& a_{k,d} + r_d + w, \end{aligned} \quad (21)$$

for $k = 1, \ldots, L_d$, and $d = 1, \ldots, D$, and $z_{2,k,d}$, $z_{1,d}$ and z_0 are independently and identically distributed (i.i.d.) Gaussian RVs with mean 0 and variance V_γ. Also, $w \sim \mathcal{N}(E_\gamma, V_\gamma \rho_0)$, $r_d \sim \mathcal{N}(0, V_\gamma(\rho_1 - \rho_0))$ and $a_{k,d} \sim \mathcal{N}(0, V_\gamma(1-\rho_1))$ for $k = 1, \ldots, L_d$ and $d = 1, \ldots, D$, are independently distributed.

The maximum of the channel parameter $\hat{\gamma}_{k,d}$ in each block is $\hat{\gamma}_d^* = \max_{k\in\{1,\ldots,L_d\}} \hat{\gamma}_k^*$ for $d = 1, \ldots, D$, and the CDF of RV $\hat{\gamma}^* = \max_{d\in\{1,\ldots,D\}} \hat{\gamma}_d^*$ can be computed as

$$F_{\hat{\gamma}^*}(y) = \mathbf{E}_w \left[\prod_{d=1}^{D} F_{\hat{\gamma}_d^*|w}(y) \right]. \quad (22)$$

Applying the PDFs of RVs $a_{k,d}$, r_d and w, that is

$$f_{a_{k,d}}(x) = \frac{1}{\sqrt{2\pi V_\gamma(1-\rho_1)}} e^{-\frac{x^2}{2V_\gamma(1-\rho_1)}}, \quad (23)$$

$$f_{r_d}(x_d) = \frac{1}{\sqrt{2\pi V_\gamma(\rho_1-\rho_0)}} e^{-\frac{x_d^2}{2V_\gamma(\rho_1-\rho_0)}}, \quad (24)$$

$$f_w(x_0) = \frac{1}{\sqrt{2\pi V_\gamma \rho_0}} e^{-\frac{(x_0-E_\gamma)^2}{2V_\gamma\rho_0}}, \quad (25)$$

we can obtain the conditional PDF of $\hat{\gamma}_{k,d}$ for $k = 1, \ldots, L_d$ and $d = 1, \ldots, D$ with $r_d = x_d$ and $w = x_0$ as

$$f_{\hat{\gamma}_{k,d}|r_d=x_d,w=x_0}(x) = \frac{e^{-\frac{(x-x_d-x_0))^2}{2V_\gamma(1-\rho_1)}}}{\sqrt{2\pi V_\gamma(1-\rho_1)}}, \quad (26)$$

and the conditional CDF as

$$\begin{aligned} &F_{\hat{\gamma}_{k,d}|r_d=x_d,w=x_0}(y) \\ &= \int_{-\infty}^{y} f_{\gamma_{k,d}|r_d=x_d,w=x_0}(x) dx \\ &= \frac{1}{2}\left[1 + \text{erf}\left(\frac{y - x_d - x_0)}{\sqrt{2\pi V_\gamma(1-\rho_1)}}\right)\right], \end{aligned} \quad (27)$$

where $\text{erf}(x)$ is the error function. Taking the expectation of $F_{\gamma_{k,d}|r_d=x_d,w=x_0}(y)$ over RV r_d, we obtain

$$F_{\hat{\gamma}_d^*|w=x_0}(y) = \int_{-\infty}^{\infty} \left(F_{\gamma_{k,d}|r_d=x_d,w=x_0}(y)\right)^{L_d} f_{r_d}(x_d) dx_d. \quad (28)$$

Finally, we can achieve

$$\begin{aligned}
&F_{\tilde{\gamma}^*}(y)\\
&=\int_{-\infty}^{\infty}\prod_{d=1}^{D}F_{\tilde{\gamma}_d^*|w=x_0}(y)f_w(x_0)dx_0\\
&=\int_{-\infty}^{\infty}\prod_{d=1}^{D}\int_{-\infty}^{\infty}\frac{1}{2^{L_d}}\left[1+\mathrm{erf}\left(\frac{y-x_d-x_0}{\sqrt{2\pi V_\gamma(1-\rho_1)}}\right)\right]^{L_d}\\
&\quad\times f_{r_d}(x_d)dx_d f_w(x_0)dx_0\\
&\approx\frac{H\pi}{U^2V_\gamma}\sum_{l=1}^{U}\prod_{d=1}^{D}\sum_{t_d=1}^{U}\frac{\left[1+\mathrm{erf}\left(\frac{y-Hp_{t,d}-Hq_l}{\sqrt{2\pi V_\gamma(1-\rho_1)}}\right)\right]^{L_d}}{2^{L_d+1}}\\
&\quad\times\sqrt{\frac{(1-p_{t,d}^2)(1-q_l^2)}{\rho_0(\rho_1-\rho_0)}}e^{-\frac{(Hp_{t,d})^2}{2V_\gamma(\rho_1-\rho_0)}-\frac{(Hq_l-E_\gamma)^2}{2V_\gamma\rho_0}},
\end{aligned}\tag{29}$$

where the Gauss-Chebyshev integral is applied in the approximation of the final step [25], H is a large number, U is a number to tradeoff accuracy and complexity, and

$$p_{t,d}=\cos\left(\frac{(2t_d-1)\pi}{2U}\right),\ \text{and}\ q_l=\cos\left(\frac{(2l-1)\pi}{2U}\right).\tag{30}$$

C. CLT and I.I.D. Channel Approximation

To gain further insight, we consider the setting that μ is close to 1 with $\mu\to 1$, and hence $\eta(\mu)\to 1$, and the block-correlation channels can be viewed as D i.i.d. channels. Thus, in the approximated channel model, we have

$$\tilde{\gamma}_k=\sqrt{1-\rho_0}b_k+\sqrt{\rho_0}b_0+E_\gamma,\tag{31}$$

where $b_k\sim\mathcal{N}(0,V_\gamma)$ for $k=0,1,\ldots,D$. Also, the PDF of b_k is given by

$$f_{b_k}(x)=\frac{1}{\sqrt{2\pi V_\gamma}}e^{-\frac{x^2}{2V_\gamma}},k=0,1,\ldots,D.\tag{32}$$

Accordingly, we can write the conditional PDF of $\tilde{\gamma}_k$ with $b_0=x_0$ as

$$f_{\tilde{\gamma}_k|b_0=x_0}(x)=\frac{e^{-\frac{(x-(E_\gamma+\rho_0x_0))^2}{2V_\gamma(1-\rho_0)}}}{\sqrt{2\pi V_\gamma(1-\rho_0)}},\tag{33}$$

and correspondingly, the conditional CDF becomes

$$\begin{aligned}
F_{\tilde{\gamma}_k|b_0=x_0}(y)&=\int_{-\infty}^{y}\frac{e^{-\frac{(x-(E_\gamma+\rho_0x_0))^2}{2V_\gamma(1-\rho_0)}}}{\sqrt{2\pi V_\gamma(1-\rho_0)}}dx\\
&=\frac{1}{2}\left[1+\mathrm{erf}\left(\frac{y-(E_\gamma+\rho_0x_0)}{\sqrt{2V_\gamma(1-\rho_0)}}\right)\right].
\end{aligned}\tag{34}$$

Moreover, taking the expectation of $F_{\tilde{\gamma}_k|b_0=x_0}(y)$ over RV b_0, we can write the CDF of $\tilde{\gamma}^*$ as

$$\begin{aligned}
F_{\tilde{\gamma}^*}(y)&=\int_0^{\infty}\left[F_{\tilde{\gamma}_k|b_0=x_0}(y)\right]^D f_{b_0}(x_0)dx_0\\
&\approx\frac{H\pi}{U}\sum_{l=1}^{U}\frac{1}{2^D}\left[1+\mathrm{erf}\left(\frac{y-E_\gamma-\rho_0Hq_l}{\sqrt{2V_\gamma(1-\rho_0)}}\right)\right]^D\\
&\quad\times\sqrt{\frac{1-q_l^2}{2\pi V_\gamma}}e^{-\frac{(Hq_l)^2}{2V_\gamma}}.
\end{aligned}\tag{35}$$

Remark 1: As can be observed, the approximate CDF of γ^* in (15) requires N-fold integration, while the approximate CDF in (29) and (34) require $(D+1)$-fold integration and one-fold integration, respectively. This indicates that the block-correlation based approximation can be effective in evaluating the performance of the FAS-RIS system, for large N.

Remark 2: From (29) and (34), we can see that the outage probability decreases with a larger D; yet the value of D may not decrease linearly with the number of FAS ports N and $D\ll N$ when the value of N is huge [20]. Therefore, it is not surprising that the enhancement brought by increasing N become less evident when N is large.

IV. Numerical Results

In this section, we provide numerical results for evaluating the outage performance of the FAS-RIS system. The distance between the BS and RIS and that between the RIS and the mobile receiver are both set to 200 meters. For path-loss factor of 2, we have $\epsilon_1=\epsilon_2=200^{-2}$. Also, $W=1$ except Fig. 3.

In Fig. 2, the variations of outage probability with different values of the number of ports N are observed, where $M=40,45$ and N varies from 5 to 50. The noise power is $\sigma_n^2=10^{-8}$ W, and the transmit power is $P_S=0.1$ W. Hence the average received SNR are $\mathbf{E}(P_S|\gamma_k|^2/\sigma^2)=10$ dB and 11.0231 dB for $M=40$ and $M=45$ respectively. The target data rate $R=3$ bit/s/Hz. In the numerical results, we give the results based on (15), (29), and (35), which are denoted as "CLT", "CLT-BC", "CLT-IID" respectively. For the block correlation model, μ is set to 0.9. For comparison, the results based on the constant correlation model in [17] are also given and denoted as "Constant". Note that [17] is not accurate.

As observed, the block-correlation model based results align well with the CLT based results, which suggests that the block-correlation model can help avoid the heavy computation of the CDF of multi-dimensional Gaussian distribution to analyze the performance of FAS-RIS systems. Also, we see that the outage probability decreases with a larger value of N, especially when the value of N is small. When the values of N is large, such as $N\geq 30$, the outage probability remains unchanged with different N. This phenomenon can also be observed from the results of the block-correlation model. However, the results of constant correlation model are much more lower than other results when the value of the number of ports N is large, which suggests that the results of constant correlation model might overestimate the system performance.

In Fig. 3, the results are provided for the outage probability with different values of W, where $M=40,45$, $N=20$ and W varies from 1 to 5. As observed, with larger values of W, the outage probability decreases, which is more obvious when $W\leq 3$. This is because when the value of W increases, the statistical dependency among the channel parameters of each port decreases, and more effective diversity can be achieved for the FAS-enabled receiver.

In Fig. 4, we plot the outage probability of FAS-RIS with different values of M, where M varies from 20 to 200, and $N=5,10$. To better demonstrate the impact of CLT on the analytical results, we scale the outage threshold Λ_{th} to E_γ.

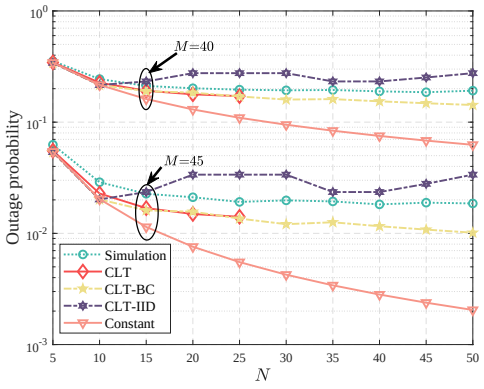

Fig. 2. Outage probability versus the number of ports N.

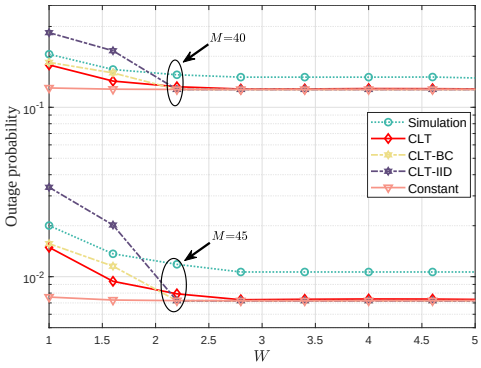

Fig. 3. Outage probability versus the number of RIS elements M.

As observed, the accuracy of the CLT based approximation results and the block-correlation based approximation results become more satisfying with large values of M.

V. Conclusions

In this correspondence, we analyzed the outage probability for FAS-RIS systems. Applying the CLT and block-correlation channel model, we derived the expressions of outage probability. Numerical results showed the effectiveness of the proposed analysis, as the derived analytical results become close to the simulation results when the number of RIS elements is large.

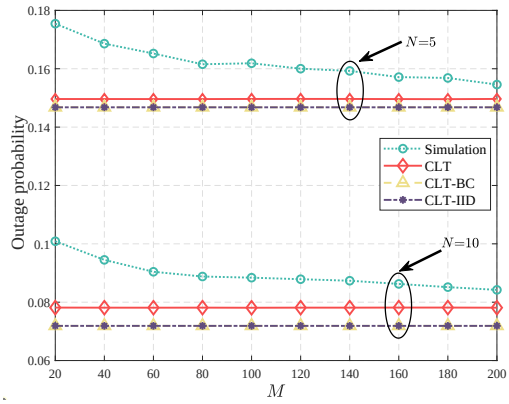

Fig. 4. Outage probability versus the number of RIS elements M.

References

[1] K.-K. Wong, A. Shojaeifard, K.-F. Tong and Y. Zhang, "Performance limits of fluid antenna systems," *IEEE Commun. Letters*, vol. 24, no. 11, pp. 2469–2472, Nov. 2020.

[2] X. Lai *et al.*, "On performance of fluid antenna system using maximum ratio combining," *IEEE Commun. Lett.*, vol. 28, no. 2, pp. 402–406, Feb. 2024.

[3] J. Zheng *et al.*, "FAS-assisted NOMA short-packet communication systems," *IEEE Trans. Veh. Technol.* , early access, doi:10.1109/TVT.2024.3363115, 2024.

[4] K.-K. Wong, K.-F. Tong, and C.-B. Chae, "Fluid antenna system—part II: Research opportunities," *IEEE Commun. Lett.*, vol. 27, no. 8, pp. 1924–1928, Aug. 2023.

[5] D. Rodrigo, B. A. Cetiner, and L. Jofre, "Frequency, radiation pattern and polarization reconfigurable antenna using a parasitic pixel layer," *IEEE Trans. Antennas & Propag.*, vol. 62, no. 6, pp. 3422–3427, Jun. 2014.

[6] Y. Huang, L. Xing, C. Song, S. Wang, and F. Elhouni, "Liquid antennas: Past, present and future," *IEEE Open J. Antennas & Propag.*, vol. 2, pp. 473–487, Mar. 2021.

[7] Z. Chai, K.-K. Wong, K.-F. Tong, Y. Chen, and Y. Zhang, "Port selection for fluid antenna systems," *IEEE Commun. Lett.*, vol. 26, no. 5, pp. 1180–1184, May 2022.

[8] N. Waqar, K.-K. Wong, K.-F. Tong, A. Sharples, and Y. Zhang, "Deep learning enabled slow fluid antenna multiple access," *IEEE Commun. Lett.*, vol. 27, no. 3, pp. 861–865, Mar. 2023.

[9] J. D. Vega-Sánchez, A. E. López-Ramírez, L. Urquiza-Aguiar and D. P. M. Osorio, "Novel expressions for the outage probability and diversity gains in fluid antenna system," *IEEE Wireless Commun. Lett.*, vol. 13, no. 2, pp. 372–376, Feb. 2024.

[10] J. D. Vega-Sánchez, L. Urquiza-Aguiar, M. C. P. Paredes and D. P. M. Osorio, "A simple method for the performance analysis of fluid antenna systems under correlated Nakagami-m fading," *IEEE Wireless Commun. Lett.*, vol. 13, no. 2, pp. 377–381, Feb. 2024.

[11] P. D. Alvim *et al.*, "On the performance of fluid antennas systems under α-μ fading channels," *IEEE Wireless Commun. Lett.*, vol. 13, no. 1, pp. 108–112, Jan. 2024.

[12] C. Psomas, P. J. Smith, H. A. Suraweera and I. Krikidis, "Continuous fluid antenna systems: Modeling and analysis," *IEEE Commun. Lett.*, vol. 27, no. 12, pp. 3370–3374, Dec. 2023.

[13] Z. Zhang, J. Zhu, L. Dai, and R. W. Heath Jr, "Successive Bayesian reconstructor for channel estimation in fluid antenna systems," arXiv preprint arXiv:2312.06551v3, 2024.

[14] J. Zhu *et al.*, "Index modulation for fluid antenna-assisted MIMO communications: System design and performance analysis," *IEEE Trans. Wireless Commun.*, early access, doi:10.1109/TWC.2024.3364712, 2024.

[15] Y. Chen, and T. Xu, "Fluid antenna index modulation communications," *IEEE Wireless Commun. Lett.*, vol. 13, no. 4, pp. 1203–1207, Apr. 2024.

[16] L. Zhu, and K. K. Wong, "Historical review of fluid antennas and movable antennas," arXiv preprint arXiv:2401.02362v2, Jan. 2024.

[17] K.-K. Wong, A. Shojaeifard, K.-F. Tong, and Y. Zhang, "Fluid antenna systems," *IEEE Trans. Wireless Commun.*, vol. 20, no. 3, pp. 1950–1962, Mar. 2021.

[18] K.-K. Wong, K. F. Tong, Y. Chen, and Y. Zhang, "Closed-form expressions for spatial correlation parameters for performance analysis of fluid antenna systems," *IET Electron. Lett.*, vol. 58, no. 11, pp. 454–457, May 2022.

[19] M. Khammassi, A. Kammoun and M.-S. Alouini, "A new analytical approximation of the fluid antenna system channel," *IEEE Trans. Wireless Commun.*, vol. 22, no. 12, pp. 8843–8858, Dec. 2023.

[20] P. Ramirez-Espinosa, D. Morales-Jimenez and K. K. Wong, "A new spatial block-correlation model for fluid antenna systems," arXiv:2401.04513v2, Jan. 2024.

[21] T. Wu *et al.*, "Fingerprint-based mmWave positioning system aided by reconfigurable intelligent surface," *IEEE Wireless Commun. Lett.*, vol. 12, no. 8, pp. 1379–1383, Aug. 2023.

[22] T. Wu *et al.*, "Exploit high-dimensional RIS information to localization: What is the impact of faulty element?," arXiv:2403.16529, Mar. 2024.

[23] L. Yang, Y. Yang, M. O. Hasna, and M.-S. Alouini, "Coverage, probability of SNR gain, and DOR analysis of RIS-aided communication systems," *IEEE Wireless Commun. Lett.*, vol. 9, no. 8, pp. 1268–1272, Aug. 2020.

[24] X. Gan, C. Zhong, Y. Zhu and Z Zhong, "User selection in reconfigurable intelligent surface assisted communication systems," *IEEE Commun. Lett.*, vol. 25, no. 4, pp. 1353–1357, Apr. 2020.

[25] E. Suli and D. F. Mayers, *An Introduction to Numerical Ananlysis*. Cambridge, U.K.: Cambridge Univ. Press, 2003.